



UNIVERSITY OF LEEDS

This is a repository copy of *Quantifying the effects of scale and heterogeneity on the confined strength of micro-defected rocks*.

White Rose Research Online URL for this paper:
<http://eprints.whiterose.ac.uk/125832/>

Version: Accepted Version

Article:

Stavrou, A and Murphy, W orcid.org/0000-0002-7392-1527 (2018) Quantifying the effects of scale and heterogeneity on the confined strength of micro-defected rocks. *International Journal of Rock Mechanics and Minings Sciences*, 102. pp. 131-143. ISSN 1365-1609

<https://doi.org/10.1016/j.ijrmms.2018.01.019>

Crown Copyright © 2018, Elsevier. This manuscript version is made available under the CC-BY-NC-ND 4.0 license <http://creativecommons.org/licenses/by-nc-nd/4.0/>

Reuse

This article is distributed under the terms of the Creative Commons Attribution-NonCommercial-NoDerivs (CC BY-NC-ND) licence. This licence only allows you to download this work and share it with others as long as you credit the authors, but you can't change the article in any way or use it commercially. More information and the full terms of the licence here: <https://creativecommons.org/licenses/>

Takedown

If you consider content in White Rose Research Online to be in breach of UK law, please notify us by emailing eprints@whiterose.ac.uk including the URL of the record and the reason for the withdrawal request.



eprints@whiterose.ac.uk
<https://eprints.whiterose.ac.uk/>

Quantifying the effects of scale and heterogeneity on the confined strength of micro-defected rocks

A. Stavrou^{1,2} and W. Murphy²

¹ Arup, 13 Fitzroy Street London W1T 4BQ United Kingdom.

² School of Earth and Environment, University of Leeds, Leeds. LS2 9JT.

ABSTRACT

Rock block strength is one of the predominant factors controlling rock mass behaviour and the response of the structural elements used as rock reinforcement. In uniaxial compression, the strength of rock blocks has been shown to be size dependent but due to practical difficulties in performing large-scale triaxial compression tests it is very difficult to quantify their *in-situ* confined strength. For that reason, a numerical study was performed to develop a framework for estimating the confined strength of rock blocks considering scale effects and *in-situ* heterogeneity (i.e. intensity of structural microdefects and degree of weathering). Grain boundary models using the Voronoi tessellation scheme within UDEC have been used to simulate the results of small (lab) and large (field) scale compression (unconfined and triaxial) and indirect tensile (Brazilian) tests on a series of progressively larger in size and degrading in quality numerical specimens. Accordingly, relationships that link rock block strength with its volume and *in-situ* condition were developed for the preliminary estimation of scaled Mohr-Coulomb and Hoek-Brown parameters.

The results from the scaling analysis generally suggest that cohesion decreases with both increasing scale and degrading sample condition in a manner similar to the scale/condition dependant reduction of uniaxial compression strength (UCS), while the friction angle shows only minor variation with no apparent trend. The measured peak confined strength values were also fitted to the Generalized Hoek-Brown criterion and a new block-scale Geological Strength Index parameter is introduced named micro GSI (mGSI) which was also linked to the scale/condition dependant reduction of UCS. By using the proposed linear and non-linear approaches, once the UCS reduction due to scaling effects is known, the confined strength of rock blocks could be then defined and can be used to carry out preliminary rock engineering calculations and especially to run discontinuum numerical models where rock blocks are simulated explicitly and represent an essential element of the analysis.

Keywords: rock block, scale effect, heterogeneity, confined strength, UDEC Voronoi

1. INTRODUCTION

In rock engineering the performance of a jointed rock mass and the interactions with rock reinforcement elements are controlled by the strength and structural pattern of discontinuities and the strength of rock blocks between the fracture networks. There is a recognised problem associated with upscaling the results of small-scale tests on both rock joints and rock blocks. This challenge in assigning parameters for use in rock engineering design and numerical modelling is made more difficult by the limited availability of large-scale tests and the practical difficulties in attempting to investigate the confined strength of larger rock block volumes. Therefore, this has historically been treated by using empirical relationships between lab scale samples and representative sizes of blocks or discontinuities, field observations and more recently by sophisticated synthetic rock mass modelling techniques¹.

If we exclude the cases where a rock mass can be represented as an equivalent continuum medium (c. 20% of cases) due to the high density or absence of fractures relative to the size of the excavation, it is clear that rock blocks and joints must be treated explicitly and a reasoned attempt to upscale their strength from small sample to field scale is required².

While there are upscaling relationships for rock joints (e.g.³), the options available to scale the strength of rock blocks are more limited (see⁴). Generic relationships that correlate the confined strength of rock blocks according to their size and *in-situ* condition are not comprehensively available in the technical literature, due to challenges associated with performing large-scale triaxial compression tests on large scale rock block volumes. For that reason, a series of small and large-scale micromechanical numerical simulations of standard tests (i.e. uniaxial/triaxial compression and indirect tensile strength) have been conducted within UDEC to establish a methodology for estimating the confined strength of rock blocks based on their volume and *in-situ* condition (i.e. degree of heterogeneity and alteration). Accordingly, relationships that link rock block strength with its volume and *in-situ* condition were developed for the preliminary estimation of scaled Mohr-Coulomb and Hoek-Brown parameters for use in discontinuum numerical modelling and rock engineering design calculations.

Given that the block scaling effects and the variable strength of defected and non-defected rock blocks is one of the predominant factors controlling rock mass behaviour⁵, the extend of the disturbed zone around an excavation⁶ and the response of the structural elements used as support⁷, the overall aim of this paper is to contribute towards a more precise prediction of rock mass strength.

2. ROCK BLOCK SCALING EFFECTS

It has been proven experimentally that the uniaxial compressive strength (UCS) of intact rock decreases with increasing sample size⁸. This has been attributed to the increased heterogeneity in rock as a function of volume and the greater probability of microdefects to allow unstable crack propagation⁹. This argument coincides with the statistical theory of¹⁰ which ascribes failure to the increased population of randomly distributed structural flaws. In contrast, some other researchers¹¹ have linked the complex size-dependent strength reduction to the combined effect of increased volume and the elevated strain energy that is stored in larger samples. Finally, Carpinteri¹² proposed that strength size effects are related to the geometrical multifractality of the fracture surfaces. Regardless of which model is accepted, the fact that larger rock blocks have observably smaller strengths than a smaller block in the same material has been established, although some exceptions have also been reported¹³. The inverse relationship between strength and size is more pronounced in materials associated with brittle behavior and appears to disappear in comparatively ductile materials. Equally in higher confining pressure tests the block size effect decrease or even vanish^{14,15}. This likely to be an effect of closure of defects that control strength at low confining pressures.

The scale-effect relationship between strength and specimen size has been validated through laboratory and *in-situ* tests for a wide range of lithological formations and several empirical and theoretical expressions have been proposed in the past in order to quantify this relationship (inter alia¹⁶⁻¹⁹).

The majority of experiments investigating scaling effects were performed under unconfined compression conditions, therefore existing scale-effect relationships are limited to the prediction of the UCS. The most widely utilised size-effect relationship was proposed by Hoek and Brown²⁰, who compiled and analysed published laboratory test data and suggested a power law function as follows,

$$\sigma_{cd} = \sigma_{c.50} \left(\frac{d}{50} \right)^{-0.18} \quad (1)$$

where $\sigma_{c.50}$ is the UCS of a 50 mm diameter cylindrical sample and σ_{cd} is the UCS of a specimen with a diameter d between 10 and 200 mm.

The dataset used by Hoek and Brown²⁰ illustrates that the rock strength reduction due to scale effects is limited by an asymptotic constant value of approximately 0.8. However, these data represent homogeneous samples and in this respect, Equation 1 is likely to over-predict the strength of samples which contain microdefects or influenced by weathering^{21,22}. In addition, Equation 1 is

applicable only for samples with diameter less than 200 mm and is only representative of medium to very strong rocks (UCS between 25-250 MPa).

In the absence of an universal strength-size law that has the ability to incorporate the variability of the *in-situ* block conditions (e.g. lithology, intensity of structural microdefects and degree of weathering) over a wide range of unjointed specimen sizes and shapes, Yoshinaka et al.²³ derived an expression that utilises an equivalent length, $d_e = V^{1/3}$, and an exponent, $k = 3/m$, as follows,

$$\frac{\sigma_c}{\sigma_{c.0}} = \left(\frac{d_e}{d_{e0}} \right)^{-k} \quad (2)$$

where m is a material constant and $d_{e0} = 62.6$ mm is the equivalent length of a specimen with a diameter of 50 mm and a ratio length to diameter equal to 2.5.

This expression follows the general form of the Hoek and Brown's equation but is using a variable exponent k and an equivalent length in order to capture the strength-scale effects for a wide range of lithologies, conditions and specimen geometries. Based on data from both laboratory and in-situ experiments, it was suggested that the exponent k varies substantially with rock type, strength and material micro-structural heterogeneity and lies between 0.1-0.3 for homogeneous strong rocks with UCS between 25-250 MPa; between 0.3-0.9 for highly weathered and/or severely microflawed rocks and between 0.0-0.5 for weak rocks with a UCS between 0.5-25 MPa (Figure 1).

From the graph shown in Figure 1, an equivalent length (≈ 200 - 250 mm) can be reached beyond which the scale effects become much less pronounced and the strength becomes independent of the specimen size and the density of defects. That critical size, is commonly referred as Representative Elementary Volume (REV) and is the minimum volume needed to evaluate the scale effects on intact rock strength⁸. The strength of a material with dimensions equal to the REV can have a minimum asymptotic value as low as about 20% of the strength measured at standard small-scale laboratory specimens.

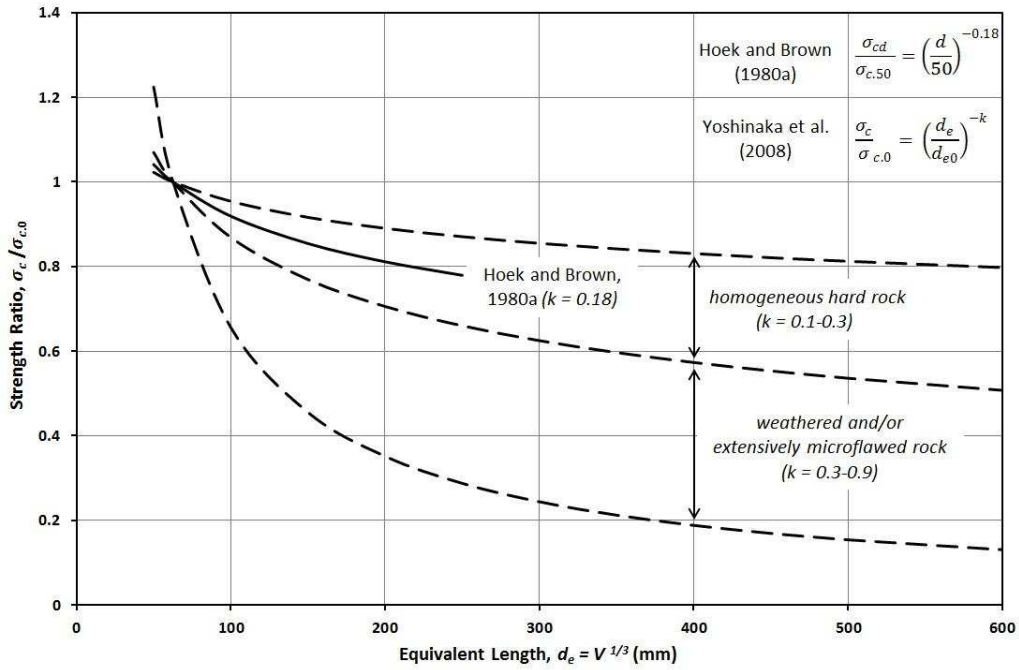


Figure 1. Scale effect relations for intact rock UCS proposed by Yoshinaka et al.²³ for sample dimensions 50 x 125 mm. The relation of Hoek and Brown²⁰ is also shown for comparison (after²¹).

3. NUMERICAL MODELLING APPROACH

3.1. UDEC micro-mechanical Damage Model

In order to develop a relationship between block size, rock *in-situ* conditions and strength, a numerical scaling approach was followed by using the Universal Distinct Element Code (UDEC) version 6.0 available from Itasca Consulting Group, Inc.

Typically, a rock block in UDEC is represented as a continuous deformable medium that indirectly mimics damage according to a chosen constitutive law. However, by using the Voronoi Tessellation Generator, a rock block can be represented as a packing of randomly-sized rigid or deformable polygonal sub-blocks which are bonded together at their contacts^{24,25}. The UDEC Voronoi model is often referred as UDEC Damage Model (DM) or Grain based Model (GBM) and represents a valuable numerical tool to build the micro-structure of rock and thus to investigate the fundamentals mechanisms of progressive damage^{26,27}. Based on this capability, the UDEC-DM is classified as a direct modelling technique in which the randomly-sized cemented polygons are linked to the grain-interface or grain cementation properties of crystalline and sedimentary rocks^{28,29}. The major advantage of the GBM direct logic against the indirect continuum modelling approach is the explicit generation and propagation of both micro-fractures and macro-fractures and that relatively simple constitutive behavior can closely resemble naturally occurring failure processes by avoiding the application of complex constitutive laws³⁰.

3.2. UDEC-DM Mechanical Behaviour

In a UDEC-DM the rock material is treated as an assembly of glued structural units interacting at their boundaries²⁹. These polygons can be assumed to represent mineral grains while their boundaries can be considered as flaws. Pre-existing cracks can also be incorporated either by the assignment of specific properties across the Voronoi grains or by the generation of micro-joints within the Voronoi skeleton^{25,31}. Because it is known that the size and size distribution of grains and flaws influence strength³², it is critical that the model resolution is sufficient enough to replicate the material behaviour and the anticipated failure mechanisms^{24,28,33}. The mechanical behaviour of a UDEC Voronoi model is therefore governed by the grain-cement micro-properties and the packing arrangement of the grains. The Voronoi micro-mechanical properties (see Table 1) refer to the deformability properties of the Voronoi sub-blocks together with the strength and stiffness parameters of the contacts that separate them.

Table 1. UDEC Voronoi micro-properties

Young's Modulus	E_m	Voronoi block elastic properties
Poisson's Ratio	ν_m	
Normal Stiffness	k_n	Voronoi contact elastic properties
Shear Stiffness	k_s	
Cohesion*	c_m	Voronoi contact strength properties
Friction Angle*	φ_m	
Tensile Strength*	t_m	
*both peak and residual properties		

The Voronoi sub-blocks are assumed to represent an equivalent elastic continuum which is sub-divided with triangular shaped finite difference zones. As a result, plastic deformation and slip or separations (i.e. damage) are confined only along the boundaries between the micro-blocks, which represent the location of potential failure paths (i.e. fractures).

The Voronoi contact behaviour will obey a linearly elastic-perfectly plastic model. The deformability of the contacts in the normal and shear directions is represented by normal (k_n) and shear (k_s) stiffnesses respectively. The shear strength of the Voronoi joints follows the MC plasticity criterion, by a combination of contact cohesion (c_m) and friction angle (φ_m), and the tensile yield is evaluated based on a limiting tensile strength (t_m). Once a force exceeds either in shear or in tension the strength of a contact, a displacement-softening procedure is followed and the shear/tensile strengths decrease to a residual value³⁴. Figure 2 illustrates the UDEC Voronoi assembly micro-properties and constitutive contact behaviour.

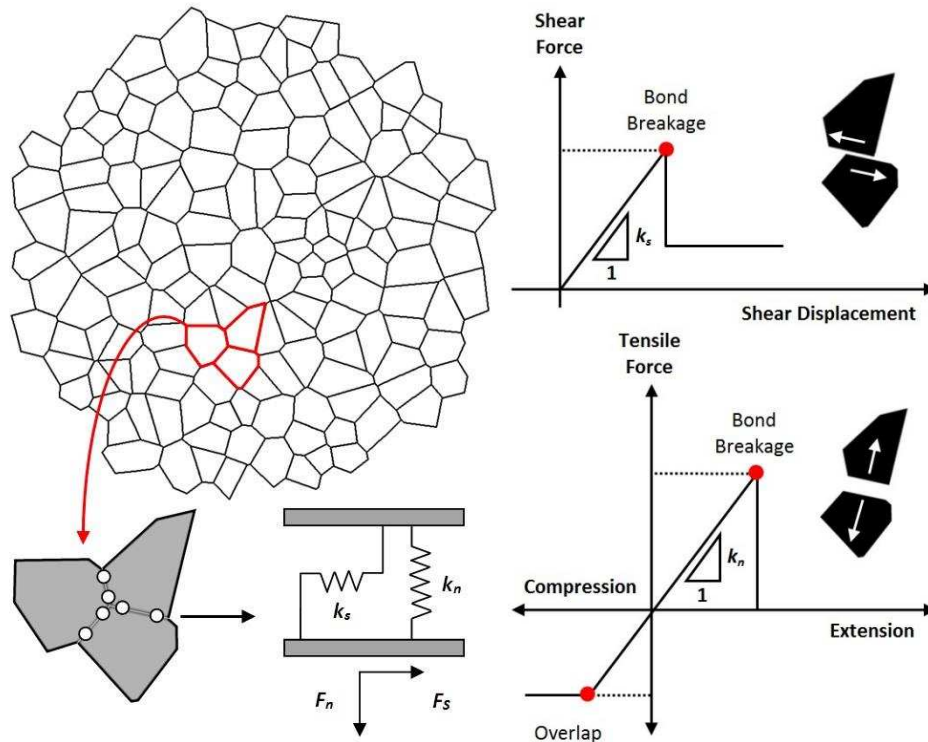


Figure 2. Structure, micro-mechanical properties and constitutive behaviour of UDEC-DM model.

When a perturbation is induced by the application of a load, a series of mechanical interactions occur between the Voronoi sub-blocks which lead in the development and transmission of contact forces, the generation of a complex heterogeneous stresses and eventually the motion and disturbance of the system. If the induced contact forces acting on and along between grain boundaries exceed their tensile or shear strength, the bond between the grains break and a compression-induced tensile or sliding crack is initiated²⁴. Redistribution of forces may then trigger stress localisations and adjacent joint breakage which, in turn, can induce microcrack propagation, interaction and the eventual generation of macroscopic failure bands²⁸. In this way, the GBM model allows the realistic fracturing of the intact rock by following the widely accepted gradual failure processes and replicates realistically the fundamental role of micro-scale tensile or extensional damage in the development of macro-fractures³⁰.

4. ROCK BLOCK SCALING METHODOLOGY

4.1. General Approach

Several numerical investigations have been conducted to study the influence of scaling effects on defected and non-defected rock blocks^{1,21,22,30,33,35-39}. A series of progressively larger micro-mechanical models were generated in UDEC and then, a series of simulated uniaxial, triaxial and indirect tensile (Brazilian) compression tests were conducted to replicate the results of small

(lab) and large (field) scale testing and subsequently to determine the relationship between size, quality and strength mechanical properties (both equivalent MC and HB).

The strength scaling analysis followed three steps:

Step 1: Estimation of typical laboratory scale macro-mechanical properties to be used as target values for the calibration of laboratory scale UDEC-DMs.

Step 2: Generation of standard laboratory size samples and simulation of standard laboratory scale tests. At this stage, the micro-mechanical properties of the GBM were calibrated via parametric analysis against the target macro-properties determined in the previous step.

Step 3: Large size UDEC-DMs were created for the simulation of large-scale testing. The micro-properties of the large GBM were initially calibrated to match a set of target uniaxial and tensile strength properties that were obtained by scaling down the strength properties of the intact rock samples considering the relation proposed by Yoshinaka et al.²³. Then, a series of large triaxial tests were performed to calculate the scaled MC and HB failure parameters.

4.2. Intact Rock macro-mechanical Properties

Two unconfined compressive strength values; 25 and 200 MPa, were selected to characterise the strength of two laboratory scale samples. These two end members cover the range of rock materials found by Yoshinaka et al. (2008) and others to be severely influenced by strong strength-scaling effects. Their macro-strength failure envelopes were determined by fitting the HB failure surface over a limited range of confining pressures (i.e. $0 \leq \sigma'_3 \leq \text{UCS}/10$). The generalised HB failure criterion⁴⁰ is described by:

$$\sigma'_1 = \sigma'_3 + \sigma_{ci} \left(m_i \frac{\sigma'_3}{\sigma_{ci}} + s \right)^a \quad (3)$$

where σ'_1 and σ'_3 are the major and minor effective principal stresses at failure, σ_{ci} is the UCS of the intact rock and m_i and s are material constants, where $s = 1$ and $a = 0.5$ for intact rock. The failure envelopes were constructed by using the σ_{ci} values of 25 and 200 MPa and by assuming a HB constant m_i equal to 10 and 30 respectively.

Equivalent MC angles of friction (φ) and cohesive strengths (c) were estimated by fitting a mean straight line to the non-linear curve defined by Equation 3. A secant envelope was defined by the peak strength σ_f and for confinements in the range P_0 (0 MPa) to P_1 ($\sigma'_3 = \text{UCS}/10$) via,

$$N_\varphi = \frac{\sigma_f(P_1) - \sigma_f(P_0)}{P_1 - P_0} \quad (4)$$

while the friction angle (φ) and cohesion (c) were obtained using²⁸,

$$\varphi = \sin^{-1} \left(\frac{N_\varphi - 1}{N_\varphi + 1} \right) \quad (5)$$

$$c = \frac{\sigma_{ci}}{2\sqrt{N_\varphi}} \quad (6)$$

The tensile strength σ_t was determined by using a relationship between the tension cutoff (defined by the ratio $\sigma_{ci}/|\sigma_t|$) and the HB parameter m_i as follows⁴¹,

$$\frac{\sigma_{ci}}{|\sigma_t|} = 8.62 + 0.7m_i \quad (7)$$

Finally, a Poisson's ratio, ν_i , equal to 0.25 was assumed for both samples and the associated intact rock Young's modulus values, E_i , were derived based on the following empirical relationship⁴²,

$$E_i = MR \sigma_{ci} \quad (8)$$

where MR is the modulus ratio, assumed to be equal to 400.

Table 2 lists the intact rock macro-mechanical properties of both samples No.1 and No.2 (hereafter referred to as "weak" and "strong" samples) respectively. Although strength scale effects for samples with UCS less than 25 MPa have been generally found to be insignificant, the behaviour of the chosen samples can be extrapolated to lower strength categories only in the case were significant evidence of scale effects have been found for the rocks under consideration.

Table 2. Lab scale Intact Rock Macro-properties.

Property		Units	Sample	
			No.1 "weak"	No.2 "strong"
UCS	σ_{ci}	MPa	25	200
Modulus Ratio	MR	-	400	400
Young's Modulus	E_i	GPa	10	80
Poisson's ratio	ν_i	-	0.25	0.25
HB Constants	m_i	-	10	30
	s	-	1	1
	a	-	0.5	0.5
Secant Slope	N_φ	-	5.1	11.0
Cohesion	c	MPa	5.5	30.2
Friction Angle	φ	[°]	42.4	56.4
Tensile Strength	σ_t	MPa	1.6	6.8

4.3. UDEC-DM Intact Rock Calibration

Micro-mechanical Model Description

A rectangular 50 x 125 mm and a circular 50 mm in diameter samples (Figure 3) were generated in UDEC to simulate laboratory scale compression (uniaxial and triaxial) and tension (Brazilian) experiments. The grain edge length and size distribution were chosen to ensure that the Voronoi block mosaic does not control the formation and accumulation of macro-fractures²⁵. The samples were discretised into a large number of random polygons with an average edge length equal to 3 mm to avoid geometry and grain size testing constraints⁴³. The Voronoi tessellation was developed with a relatively non-uniform grain size distribution to mimic the internal micro-structural heterogeneity that is typically observed in real rocks³⁰.

All model simulation include two steel platens at the top and bottom of the samples. A constant velocity was applied in the y-direction at the upper platen while the lower platen was fixed in both the x- and y-directions. An axial loading velocity of 0.01 ms⁻¹ (i.e. loading rate) was applied to the top platen in both the compression and tension tests. The loading rate was selected to ensure that the samples remain in a quasi-static state²⁹. In the case of the triaxial tests, stresses were applied isotropically to the lateral boundaries and static equilibrium was reached prior to axial loading.

For all the simulated compression tests, the axial stress was continuously recorded by the sum of the reaction forces along the contact between the sample and the top loading platen. The axial and lateral strains were monitored at several locations across the middle one-third of the specimens (Figure 3) and then built-in FISH functions were used to calculate average strain values.

For the tension tests, the axial stress was defined by considering sum of the reaction forces that generated along an artificial joint in the middle of the upper platen. The peak axial stress was measured indirectly via,

$$\sigma_t = \frac{P_{max}}{\pi R t} \quad (9)$$

where P_{max} is the maximum force recorded on the platen, R and t symbolise the radius and thickness of the disk specimen, where t=1 for a 2D analysis.

In all models, when a force violates the strength of a contact segment (either in shear or tension), an internal plasticity flag is set to declare the irreversible plastic state of the contact, the cohesive and tensile strengths are eliminated to zero (instantaneous softening) and the friction angle is soften to a residual value.

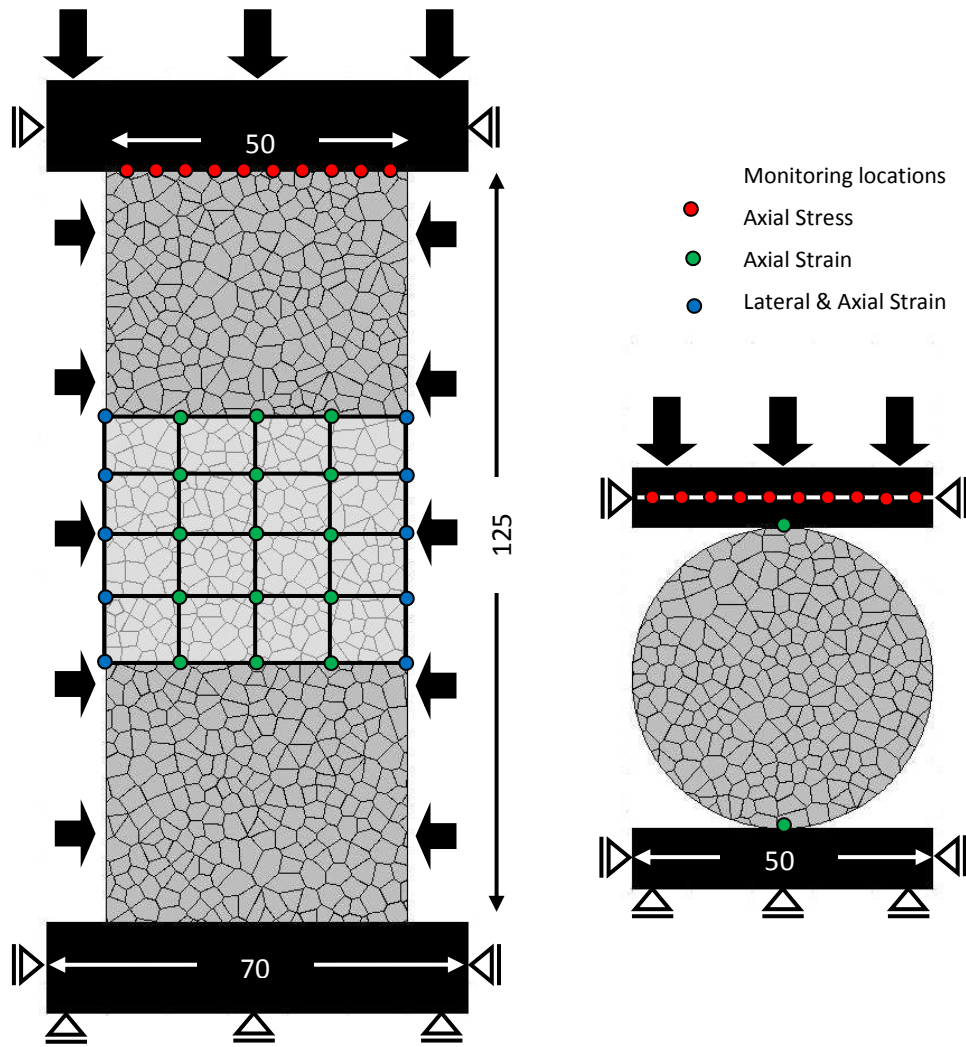


Figure 3. Layout, boundary conditions and monitoring locations (i.e. UDEC history points) of the compression and indirect tensile strength tests (COLOR).

Calibration Procedure

The micro-parameters controlling the elasticity (i.e. E_m , ν_m , k_n and k_s) and strength (i.e. c_m , φ_m and t_m) behaviour of the micro-block assembly were estimated following a multi-stage parametric analysis in which the model response was calibrated against the deformability (i.e. E_i , ν_i) and strength (i.e. c , φ and σ_t) macro-mechanical properties shown in Table 2. The trial-and-error calibration process followed the procedures outlined by Christianson et al.³³, Kazerani and Zhao²⁹ and by Gao and Stead²⁵. In summary, the following steps were followed:

Calibration - Step 1: The macro-mechanical Young's Modulus (E_i) and Poisson's ratio (ν_i) were calibrated by running a series of unconfined compression test simulations. The Young's Modulus and Poisson's ratio of the grains were initially defined to be equal to the macro-properties of the intact rock (i.e. $E_i = E_m$ and $\nu_i = \nu_m$). The macro-Poisson's ratio (ν_i) was then calibrated by varying the contact stiffness ratio k_s/k_n . Once the contact stiffness ratio was set, both the normal stiffness (k_n)

and block deformability (E_m) were altered to fit the macro-Young's Modulus (E_i). In this process, the normal stiffness (k_n) of the contacts was set to a factor times the deformability of the block zones using the following expression (Itasca, 2014),

$$k_n = n \left[\frac{K_m + (4/3) G_m}{\Delta Z_{min}} \right], 1 \leq n \leq 10 \quad 10)$$

where K_m and G_m are the bulk and shear stiffnesses of the Voronoi blocks respectively, and ΔZ_{min} is the smallest width of the zone adjoining the contact in the normal direction.

Calibration - Step 2: The material tensile strength (σ_t) was calibrated by running a series of Brazilian disk tests with varying contact micro-tensile strength (t_m).

Calibration - Step 3: The material micro-cohesion (c_m) and -friction angle (φ_m) values were calibrated by running a series of triaxial compression tests with increasing confining pressures in the range $0 \leq \sigma'_3 \leq \text{UCS}/10$. The macro-cohesion (c) was calibrated by adjusting the Voronoi contact micro-cohesion and then the macro-friction angle was (φ) calibrated by rescaling the Voronoi contact micro-friction angle.

The micro-properties produced by the described calibration process are listed in Table 3. By using the calibrated properties shown in Table 3, a perfect agreement was found to the macro-strength and -stiffness values shown in Table 2.

Table 3. Calibrated UDEC Voronoi micro-properties.

Property	Units	Sample		
		No.1 "weak"	No.2 "strong"	
Voronoi Block Elastic Properties				
Young's Modulus	E_m	GPa	7.0	58.0
Poisson's Ratio	ν_m	-	0.25	0.25
Bulk Modulus	K_m	GPa	4.7	38.7
Shear Modulus	G_m	GPa	2.8	23.2
Voronoi Contact Elastic Properties				
Normal Stiffness	k_n	GPa/m	5500	46400
Shear Stiffness	k_s	GPa/m	4125	32480
Stiffness Ratio	k_s/k_n	-	0.75	0.70
Voronoi Contact Strength Properties				
Cohesion	c_m	MPa	7.2	50.7
Friction Angle	φ_m	[o]	44.0	52.0
Tensile Strength	t_m	MPa	2.3	7.5
Residual Cohesion	c_{mr}	MPa	0.0	0.0
Residual Friction Angle	φ_{mr}	[o]	15.0	15.0
Residual Tensile Strength	t_{mr}	MPa	0.0	0.0

Figure 4 and Figure 5 provide the stress-strain response of the calibrated models and present the sample damage for different confinement pressures. The white voids within the numerical samples represent macro-fractures which were formed as a result of grain de-bonding and micro-crack coalescence. The UDEC grain-based models clearly capture the fundamental behaviours of rocks in compression tests and prove they are capable of replicating the expected

significant rock strengthening as a function of confinement and the transition from brittle to ductile behaviour from low to high confining pressures. For both the unconfined and triaxial compression tests, the stress-strain response of the samples show an initial linear elastic trend up to a peak stress value. The post-peak failure response of the specimens in uniaxial compression generally exhibits a rapid loss of strength while the stress-strain curves of the confined specimens pass progressively from a strain-softening to a strain-hardening behaviour with higher ductility as confining pressure increases. At low or no confinement the samples fails mainly due to axial splitting whereas at higher confining pressures a transition in the failure mode is observed and the models capture the development of typical macroscopic shear fractures and/or conjugate damage zones.

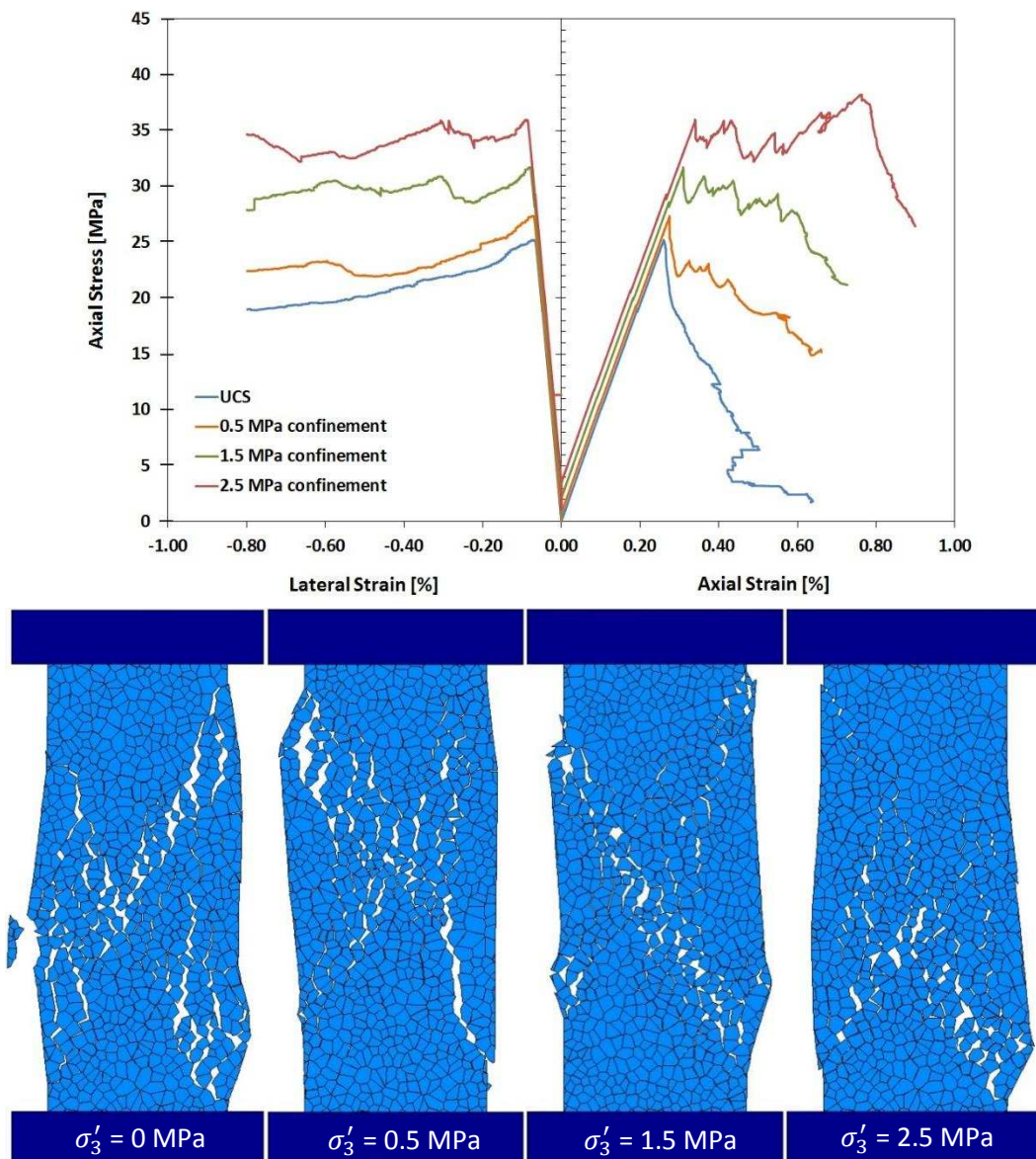


Figure 4. Sample No.1: simulated compression tests showing the calibrated stress-strain response and sample damage for different confining pressures (COLOR).

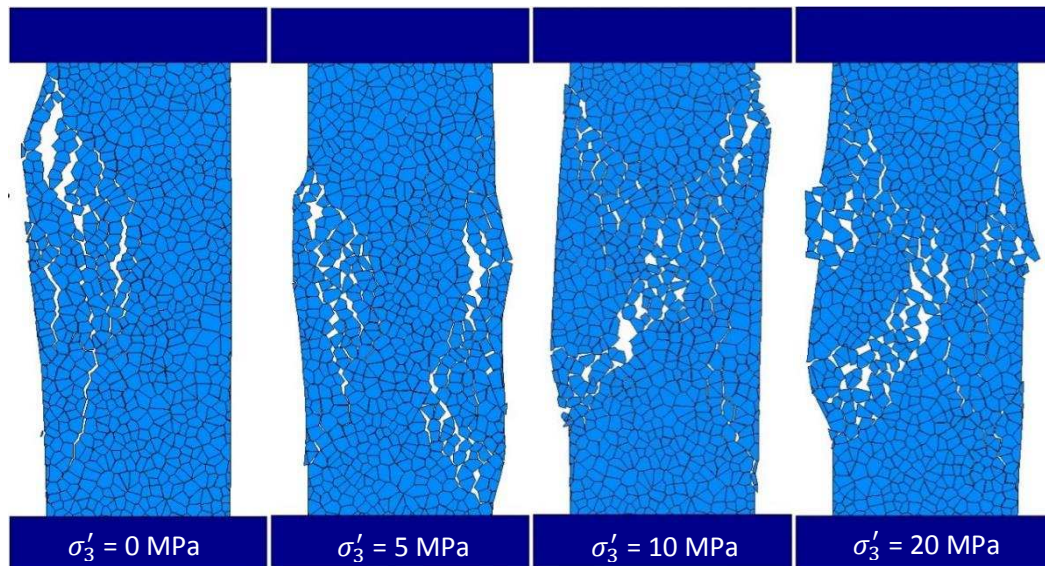
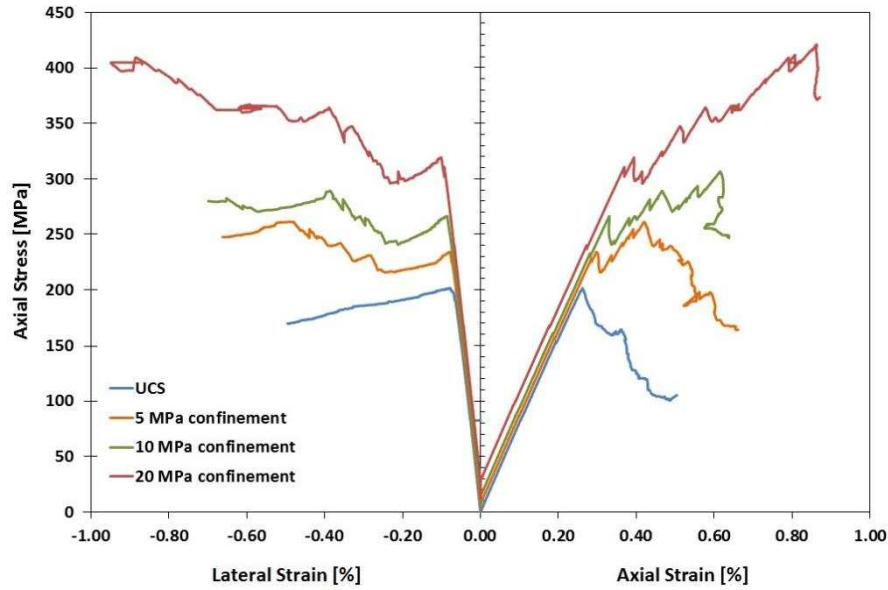


Figure 5. Sample No.2: simulated compression tests showing the calibrated stress-strain response and sample damage for different confining pressures (COLOR).

To examine the repeatability of the target values by using the calibrated micro-parameters, four different Voronoi tessellations were generated for each model and all tests were repeated following identical procedures and boundary conditions. Figure 6 show the results in a principal stress space (i.e. σ'_1 vs. σ'_3) and compare the peak stress values calculated from all the analyses with the empirical HB failure envelopes defined by Equation 3. Considering that the grain size distribution has been kept constant, it appears that numerical samples of similar “heterogeneity” produce similar results and influenced by identical failure mechanisms (i.e. extensional microcracking due to tensile stress concentrations along the grain boundaries). The relationship between the GBM results and the HB envelope clearly indicates a very good fit and gives confidence that the UDEC-DM approach is

the appropriate tool to simulate realistically large-scale uniaxial/triaxial compression and tensile tests for the needs of the scaling analysis presented in the following section.

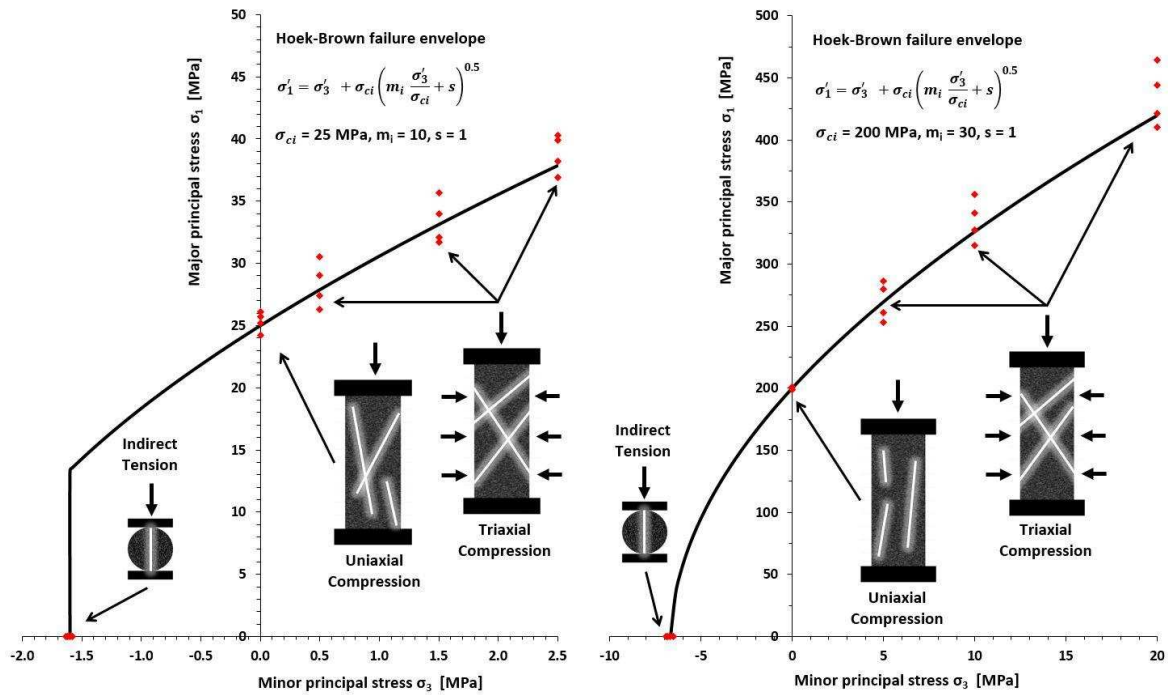


Figure 6. HB failure envelope and UDEC-DM lab-scale results for samples No.1 (left) and No.2 (right), including the typical failure mechanisms observed during modelling (COLOR).

4.4. Scaling Analysis

The numerical modelling scaling analysis procedure included three distinct steps.

Scaling Analysis - Step 1

Three progressively larger samples were chosen to be simulated in compression and indirect tension tests. These samples were 100 x 250 mm, 200 x 500 mm and 400 x 1000 mm for the compression and 100 x 100 mm, 200 x 200 mm and 400 x 400 mm for the Brazilian disk tests. The mathematical function proposed by Yoshinaka et al.²³ was adopted to predict their reduced UCS values under three different conditions (i.e. three different k exponents 0.1, 0.3 and 0.9 in Equation 2) based on increased likelihood of structural microdefect intensity and/or degree of weathering. Scaled tensile strength values were assumed to obey again on the Yoshinaka et al.²³ function whereas the macro-stiffness values were assumed to be the same for all models because deformation modulus is relatively scale independent^{18,22,44,45}. The estimated scaled uniaxial and tensile strength properties were utilised as target values that were calibrated for step 2. Table 4 shows the target reduced uniaxial compressive and tensile strength values of the three progressively larger samples as a function of the exponent k and the equivalent sample length (d_e).

Table 4. Target uniaxial compressive and tensile strength values used for the scaling analysis.

Test	width mm	height mm	volume mm ³	d_e mm	No of blocks	Sample No.1			Sample No.2			
						k			k			
						0.1	0.3	0.9	0.1	0.3	0.9	
Uniaxial Compression	50	125	2.5E05	62.6	761	σ_{ci} MPa	25.0	25.0	25.0	200.0	200.0	200.0
	100	250	2.0E06	125.2	2912		23.3	20.3	13.4	186.6	162.5	107.2
	200	500	1.6E07	250.4	11373		21.8	16.5	7.2	174.1	132.0	57.4
	400	1000	1.3E08	500.9	44971		20.3	13.4	3.8	162.5	107.2	30.8
Brazilian	50	50	4.9E04	36.6	256	σ_t MPa	1.6	1.6	1.6	6.8	6.8	6.8
	100	100	3.9E05	73.2	926		1.5	1.3	0.9	6.3	5.5	3.6
	200	200	3.1E06	146.5	3578		1.4	1.1	0.5	5.9	4.5	2.0
	400	400	2.5E07	292.9	14173		1.3	0.9	0.2	5.5	3.6	1.0

Scaling Analysis - Step 2

Three progressively larger UDEC Voronoi samples were generated by keeping the same grain size distribution characteristics. Subsequently, several uniaxial compression and Brazilian test simulations were run for each sample size to calibrate the models. During the new calibration process, the initial calibrated Voronoi contact micro-strength properties (i.e. Table 3: c_m , φ_m and t_m of models No.1 and No.2) were systematically downgraded to reach the target macro-strength values shown in Table 4 following a strength reduction approach.

The different calibrated reduced properties represent indirectly the progressive elevated disturbance of the large samples, as inferred by the variability of the exponent k in Equation 2. In general, it is considered impractical to attempt modelling explicitly the effect of pre-existing micro-structural heterogeneities (e.g. pores, flaws, cavities, fissures, veins, micro-cracks) in UDEC as long as the overall mechanical response of the models is in agreement with the overall material behavior of the disturbed samples. Figure 7 shows the calibrated stress-strain curves for the experimental simulations while Figure 8 shows examples of the failure geometries indicated in test simulations. Regardless of the size and the quality of the samples, it was shown that extensional fracturing dominates the failure process under unconfined conditions with the formation of macro-cracks parallel to the direction of loading. It should also be noted that for the models that were allowed to run for a sufficient large number of numerical cycles, shear localization was also observed and a mixed axial splitting / shear banding type of failure was captured at the final stage of the analysis.

As previously, in order to verify that the reduced micro-strength properties can reproduce the target macro-strength values, the tests were repeated under different Voronoi tessellations apart from the 400 x 1000 mm compression and 400 x 400 mm tension tests which proved to be excessively large and computationally demanding. It should be noted that the $k = 0.9$ case of the 400 x 1000 mm size models was not calibrated as was regarded to give unrealistically low strength values that can be explained only by the presence of critical orientated macro-planes of weakness^{22,46}.

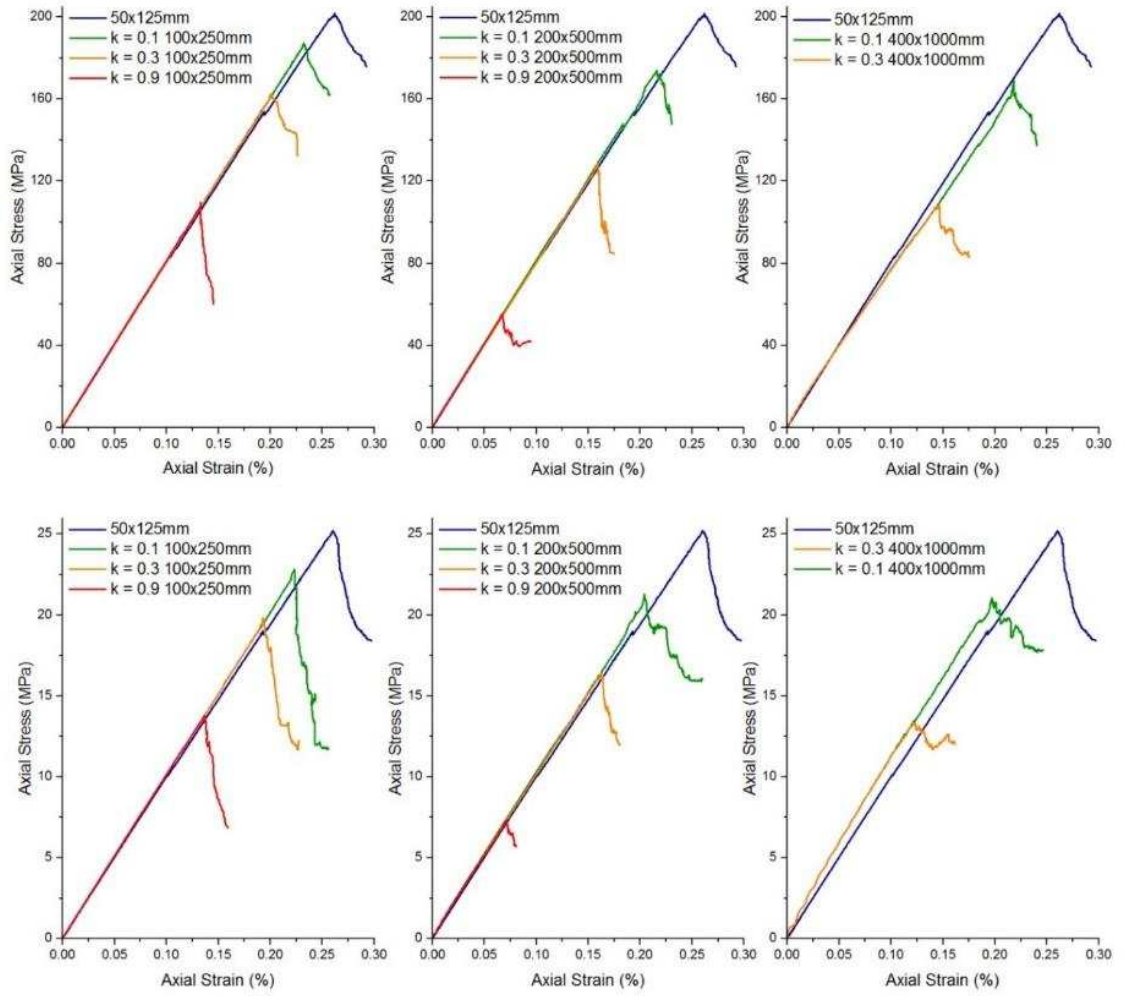
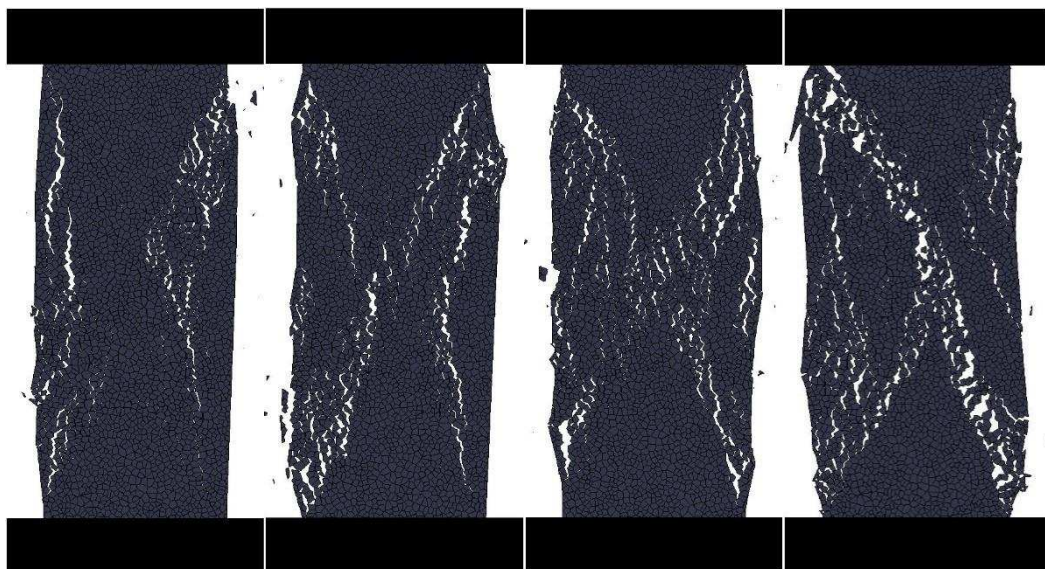


Figure 7. Calibrated stress-strain response of all sample sizes for three different physical conditions (i.e. three different k exponents 0.1, 0.3 and 0.9 in Equation 2) (COLOR).



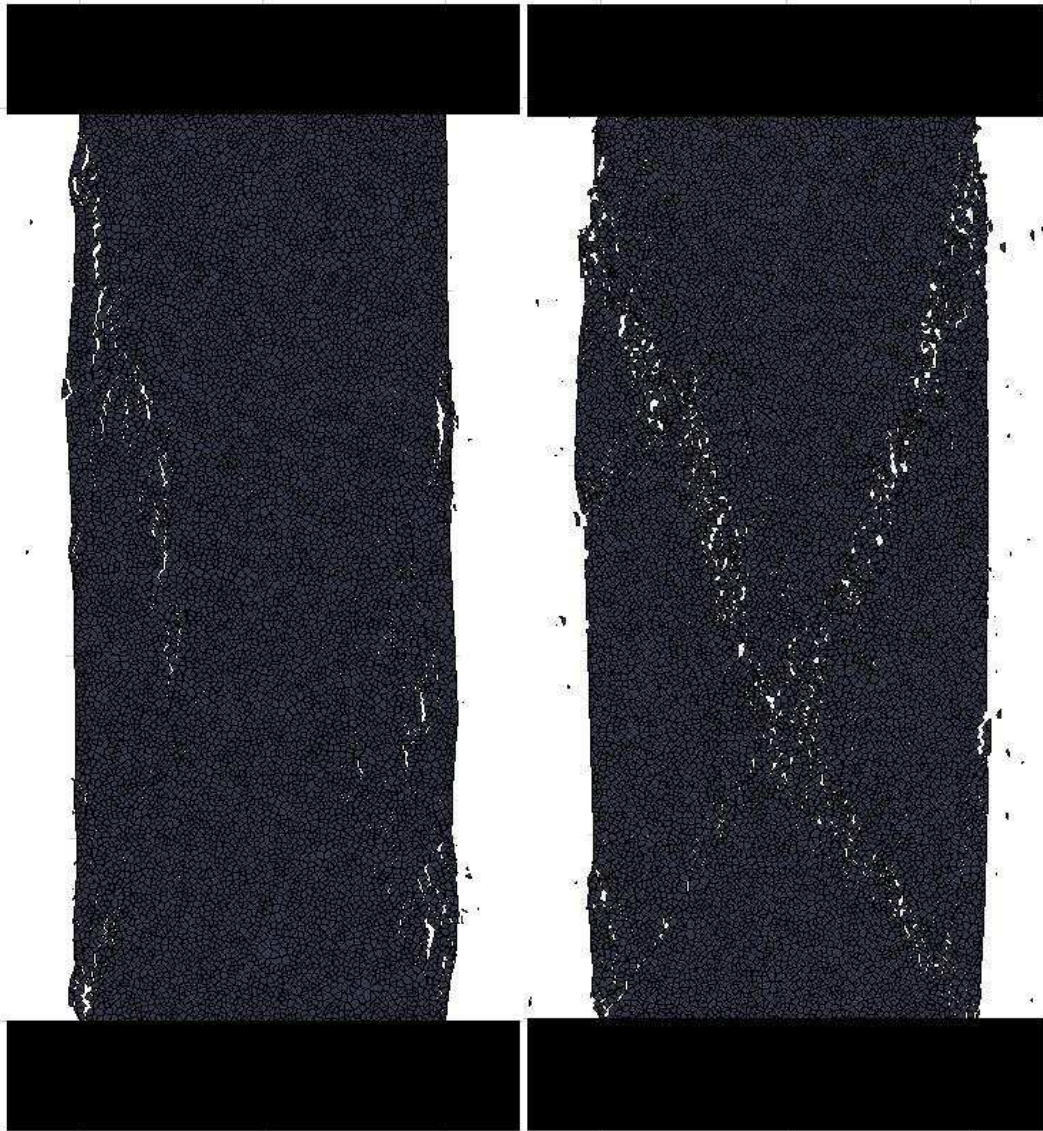


Figure 8. Examples of macroscopic axial fractures for different sample sizes and conditions during the uniaxial compression tests.

Scaling Analysis - Step 3

Once, the micro-strength properties were calibrated to match the reduced target unconfined macro-strength values (see Table 4 and Figure 7), a series of large-scale triaxial tests were performed in the 3rd step to predict scaled linear (MC) and non-linear (HB) failure envelopes. These steps allowed a methodology for estimating scaled rock block failure properties based on their volume and *in-situ* condition to be established. The confining pressures used in these analyses were in the range of $0 \leq \sigma'_3 \leq \text{UCS}/10$ and identical with those used for the calibration of the lab-scale rock samples.

The increase of sample size and disturbance reveals a strong size/condition effect to the predicted confined peak strengths values. A review of the data suggests that the rate of confined

strength decrease reduces with increasing confinement and increases with sample disturbance and size. Similarly to the lab-scale samples, macro-fracturing tends to be almost parallel with the loading direction (i.e. axial-splitting) at low confining pressures, while as confinement increases the failure modes are dominated by the formation of macroscopic shear and conjugate zones. Hence, it is once again verified that under different confining pressures, the triggered failure mechanisms are independent from the scale of the sample.

Figure 9 exhibits the predicted scaled relationship between the predicted macro-cohesion and friction angle values in respect to the specimen equivalent length (d_e). The scaling analysis results of both samples generally suggest that material macro-cohesion decreases with both increasing scale and degrading sample condition up to an asymptotic value while the macro-friction angle appears relatively insensitive. This behaviour is consistent with experimental findings given by Il'Nitskaya⁴⁷, Pratt⁴⁸, Tani⁴⁹ and Liu⁵⁰. These findings suggest that all samples have experienced the weakening of their cohesive component prior to the mobilisation of the frictional strength and that their behaviour can be captured within a Mohr-Coulomb linear logic only by a cohesion-weakening-friction-strengthening constitutive model. A review of the scale/condition dependant reduction of UCS and material cohesion shown in Figure 1 and Figure 9 respectively, reveals a similarity in the non-linear decrease of these properties and therefore suggests that Equation 2 can be transformed as follows:

$$\frac{c_c}{c_{c,0}} = \left(\frac{d_e}{d_{e0}} \right)^{-k} \quad (11)$$

where $c_{c,0}$ is the cohesion of a standard laboratory size sample and c_c is the cohesion of specimens with equivalent length d_e . Based on this observation, it means that once the UCS reduction due to scaling effects has been determined and the cohesion and friction angle of the lab-scale sample have been estimated, the block-scale cohesion can be predicted using Equation 11 while the friction is suggested to remain unchanged or altered up to $\pm 20\%$ of the original value since exhibits no clear increasing or decreasing trends.

To fit non-linear failure envelopes, all scaling analysis results were plotted in a principal stress space according to the numerical sample sizes (Figure 10). The recorded peak strength values for both the "weak" and "strong" samples display a clear pattern at each confining pressure and a consistent rock strengthening with increasing confinement, regardless of the specimen's condition or size. These results again indicate that the friction angle of large samples remains relatively unchanged while the cohesion is influenced by marked scaling and quality effects.

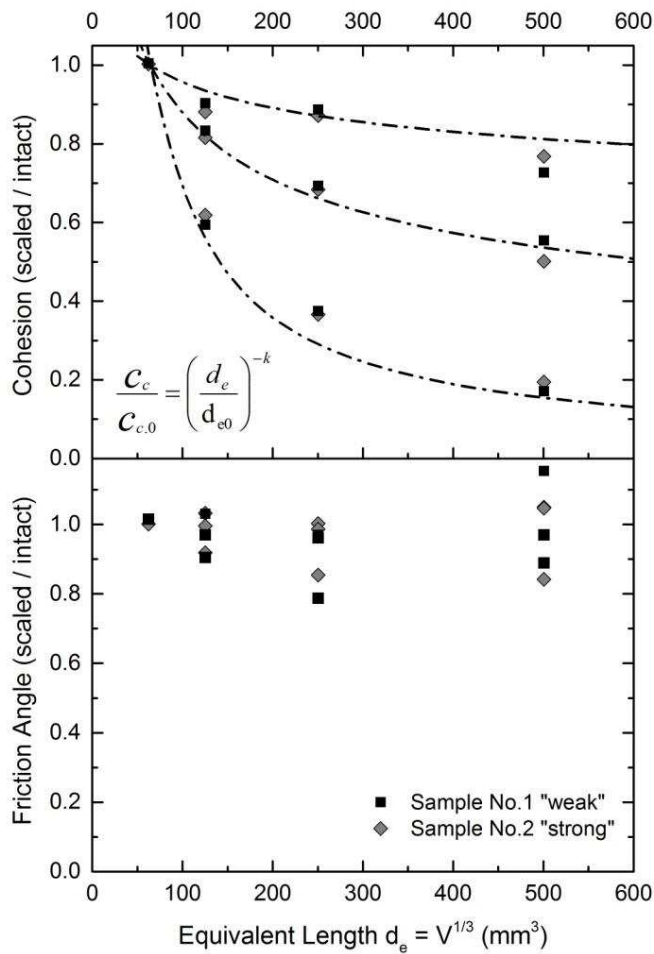


Figure 9. Predicted dimensionless relationships between material macro-cohesion and friction angle values with the specimen equivalent length.

To derive scaled strength failure envelopes, a non-linear curve fitting process was followed using the Generalized Hoek-Brown criterion and the Geological Strength Index (GSI)^{40,51}. In this process, the HB constant m_i is systematically reduced with respect to the exponent k of the Yoshinaka et al.²³ relationship, following the percentages shown in Figure 11. In essence, the GSI system is utilised as a rock block (instead of rock mass) scaling parameter to reduce the strength of the intact rock and establish a best-fit to the dataset. However, the derived GSI values could easily be linked with the internal condition (e.g. micro-heterogeneity, weathering, etc.) of the large-scale block volumes and therefore the back-calculated GSI values can be regarded to have a real physical meaning to the rock block strength reduction. For this reason, to avoid confusion with terminology, a new block-scale GSI parameter is introduced, named micro Geological Strength Index (mGSI), which can be used to predict the in-situ peak confined strength of field-scale rock blocks. The mGSI replaces the traditional GSI parameter in the HB expressions and reflects the elevated rock block disturbance with increasing scale, intensity of structural microdefects and degree of weathering.

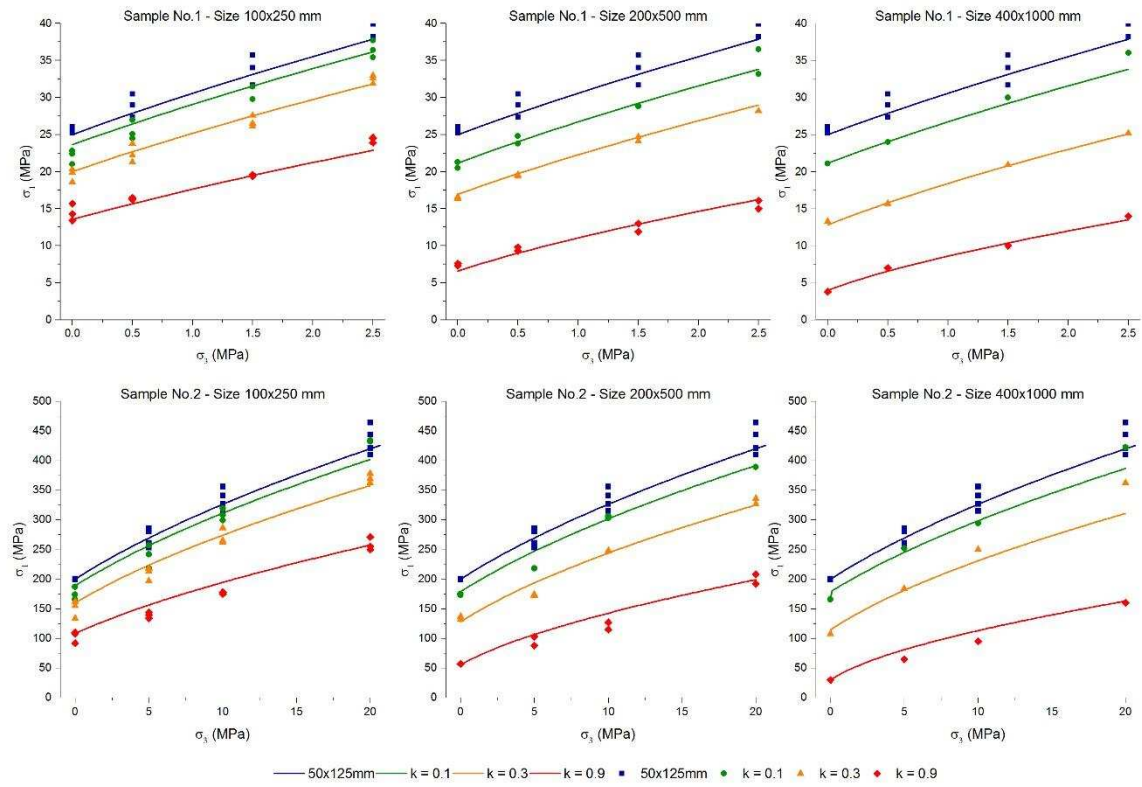


Figure 10. Measured peak strengths for samples No.1 "weak" and No.2 "strong" together with HB non-linear failure envelope fits for different physical conditions and sample sizes (COLOR).

Figure 11 shows the calibrated mGSI values against the reduced UCS of the large-scale samples, as were defined by using the function proposed by Yoshinaka et al.²³, normalised by their unconfined intact rock strength. The characteristic lab-scale UCS is advisable to be estimated from a sufficiently large number of experiments to capture strength variability as a result of localised features, damage during coring and to overcome sampling bias. The corresponding relationship to account the strength loss as a function of block volume and/or quality can be described by power-law expression and is given by,

$$mGSI = 100 \left(\frac{\sigma_c}{\sigma_{c,0}} \right)^{0.021} \quad (12)$$

From Figure 11 (or Equation 12), once the reduced UCS of the field-scale blocks is known, a mGSI value between 100 and 65 could be found and the *in-situ* confined strength of the blocks could be then estimated using the Generalized HB strength criterion. In the absence of large-scale unconfined strength tests, the user needs to decide based on geological descriptions and engineering judgment how much to reduce the UCS value of the large-scale blocks or to use the Yoshinaka et al.²³ scaling approach.

Hence, by using the proposed linear and non-linear approaches given with Equation 11 (or Figure 9) and Equation 12 (or Figure 11) respectively, a unique set of strength parameters that describe the *in-situ* strength of rock blocks could be defined, that can be used to carry out preliminary rock engineering calculations and especially to run discontinuum numerical models where rock block strength is an essential parameter of the analysis.

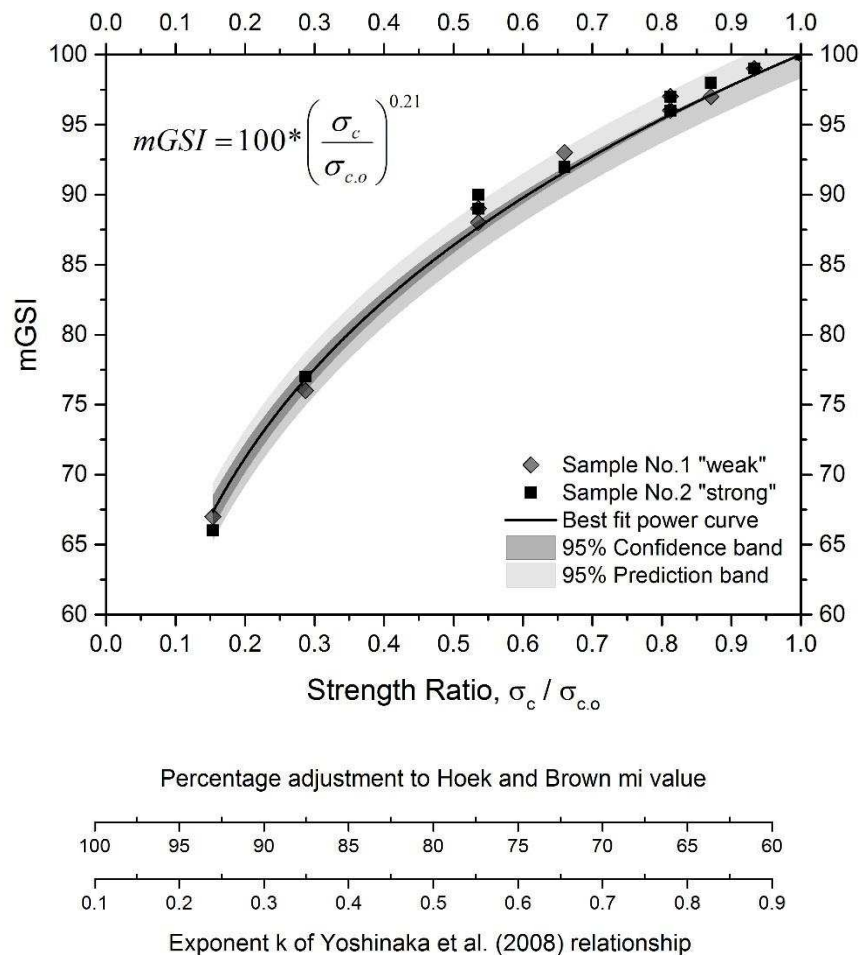


Figure 11. Predicted relationship between mGSI and the UCS strength ratio $\sigma_c / \sigma_{c,o}$ (above) and percentage adjustment to the HB mi value with respect to the k exponent of the Yoshinaka et al.²³ relationship (below).

DISCUSSION

This study examined the effect of size and heterogeneity on the confined strength of rock specimens. A series of compression and Brazilian tests were run in UDEC at progressively larger in size and degrading in quality grain-based models in order to develop a framework for estimating the confined strength of rock blocks considering scale effects and *in-situ* heterogeneity.

The results reveal that macro-cohesion is strongly influenced by both size and condition effects while the macro-friction angle shows only minor variation with no apparent trend. A comparison between the predicted cohesion and the scaled UCS values clearly demonstrates a similarity between their behaviors and appears safe to conclude that there is an inter-dependency between them. To our view, this is linked with the concept of cohesion loss and the delayed friction mobilization. Similarly to the UCS, above a critical volume the cohesion of the rock blocks becomes size-invariant and approaches a constant value. Consequently, knowledge of the scale/condition related UCS reduction can be used as a guide to define the variability of the material cohesion in larger block volumes while the friction angles are suggested to remain relatively unchanged.

Analysis of the large-scale triaxial tests data shows that there is a systematic block strength reduction with increasing specimen volume and decreasing rock quality. The HB approach was adopted to estimate the reduced peak confined strength and a new mGSI parameter is proposed to be used in the HB expressions to fit non-linear failure envelopes with a reasonable success. The predicted range of the mGSI (i.e. 100-65) describes the *in-situ* block-scale condition of individual rock pieces but further research is required to rationalise the mGSI in terms of geological characterisations or other approaches. A simple non-linear curve was fitted to approximate the relationship between mGSI and the normalised UCS strength reduction. By using this relationship, the confined strength of blocks can be estimated provided that the UCS strength ratio $\sigma_c / \sigma_{c,0}$ is known. Although appears tempting to reverse this expression (Equation 12 or Figure 11) and back-estimate the strength reduction of the rock blocks based on known mGSI values, the development of a qualitative or quantitative approach similar to the known published GSI charts is not feasible at this stage and further research is required to establish a correlation between strength, mGSI, size and the internal *in-situ* condition of the rock blocks. Despite of these difficulties, it is to be expected that the increase in the intensity of structural microdefects and/or the degree of weathering (i.e. increase of exponent k in Equation 2) will cause a reduction in the mGSI values which in turn will reduce the confined strength of the blocks under consideration.

When applying the mGSI, a rock block is assumed as an equivalent isotropic medium and is not affected by preferential anisotropy or planes of weakness. In the case of critically orientated structural features, a modified HB criterion such the one proposed by Saroglou and Tsiambaos⁵² should be used and then a scaling analysis could be performed to examine the effect of rock anisotropy in larger rock blocks.

CONCLUSIONS

Rock block strength is a significant factor controlling rock mass behaviour (i.e. deformations, failure modes, etc.) and rock-support/reinforcement interactions. Hence, a high degree of accuracy and experience is required in the estimation of rock block properties, especially when running discontinuum numerical models where rock masses are simulated as a system of rock blocks which are separated by persistent or non-persistent fracture networks.

It is well known that the lab-scale unconfined compressive strength reduces with increasing sample size and that is influenced by material quality and the presence of flaws, cavities, fissures, veins, healed joints and micro-cracks. However, because of many uncertainties and the practical difficulties in performing large-scale triaxial compression tests, generic relationships that correlate the confined strength of rock blocks with their size and condition, even in a qualitative sense, are very difficult to be established and only few studies have investigated this subject (e.g.¹⁹).

Sophisticated numerical modelling has allowed to overcome some of the practical limitations and is seen as the most effective tool for assessing the *in-situ* confined strength of rock blocks. Accordingly, a scaling analysis was performed in UDEC and based on our findings, relationships that link rock block strength with its volume and condition are proposed for the preliminary estimation of scaled Mohr-Coulomb and Hoek-Brown parameters.

The proposed predictive approaches are by no means intended to replace large scale laboratory and *in-situ* testing programs, but aims to provide the engineer and numerical analyst with a practical design tool for the preliminary estimation of size/condition related rock block strength parameters that can be used in rock mechanics numerical modelling and design. The proposed strength relationships overcome important practical difficulties and considered as very friendly tools to describe the inverse confined strength relationship as a function of scale and material quality. While limitations exist, the methodology outlined and the results obtained are considered as a significant step towards the development of a rigorous approach for estimating the confined strength of blocks and a basis for overcoming the challenge of assigning realistic parameters for blocks in discontinuum models which so far is a matter of speculation.

ACKNOWLEDGMENTS

The authors would like to thank ARUP and AECOM for financially supporting this research. Harry Saroglou and Fuqiang Gao are gratefully acknowledged for discussion and advice on matters pertaining to block scaling effects and micromechanical modelling using UDEC.

REFERENCE

1. Mas Ivars D, Pierce ME, Darcel C, et al. The synthetic rock mass approach for jointed rock mass modelling. *Int J Rock Mech Min Sci.* 2011;48(2):219-244. doi:10.1016/j.ijrmms.2010.11.014.
2. Bandis SC, Sharp JC, Mackean RA, Bacasis EA. Explicit Characterisation and Interactive Analysis for Engineering Design of Rock Caverns. In: *Proceedings of the Joint Hong Kong Institute of Engineers – Hong Kong Institute of Planning Conference on Planning and Development of Underground Space.* ; 2011:133-142.
3. Barton N, Bandis S. Effects Of Block Size On The Shear Behavior Of Jointed Rock. In: *The 23rd U.S Symposium on Rock Mechanics (USRMS).* ; 1982:739-760.
4. Bahrani N, Kaiser PK. Strength Degradation Approach (SDA) for Estimation of Confined Strength of Micro-Defected Rocks. In: *50th US Rock Mechanics / Geomechanics Symposium.* American Rock Mechanics Association; 2016.
5. Kaiser PK, Amann F, Bewick RP. Overcoming challenges of rock mass characterization for underground construction in deep mines. In: *13th ISRM International Congress of Rock Mechanics.* International Society for Rock Mechanics; 2015.
6. Shen B, Barton N. The disturbed zone around tunnels in jointed rock masses. *Int J Rock Mech Min Sci.* 1997;34(1):117-125.
7. Stavrou A, Murphy W, Lawrence JA. Evaluating the influence of block size in cable bolt performance. In: *ISRM Regional Symposium-EUROCK 2015.* International Society for Rock Mechanics; 2015.
8. Cunha AP. Scale effects in rock mechanics. In: *Proceeding of 1st International Symposium on Scale Effects in Rock Masses, Scale Effects in Rock Masses,* A. Pinto Da Cunha (Ed.), Balkema, Rotterdam. ; 1990:3-27.
9. Hoek E, Brown ET. Practical estimates of rock mass strength. *Int J Rock Mech Min Sci.* 1997;34(8):1165-1186.
10. Weibull W. A statistical distribution function of wide applicability. *J Appl Mech.* 1951;18:293-297. doi:citeulike-article-id:8491543.
11. Einstein HH, Baecher GB, Hirschfeld RC. The effect of size on strength of a brittle rock. *Int Soc Rock Mech Proc.* 1970;1(1-19).
12. Carpinteri A. Fractal nature of material microstructure and size effects on apparent mechanical properties. *Mech Mater.* 1994;18(2):89-101. doi:10.1016/0167-6636(94)00008-5.
13. Darlington WJ, Ranjith PG, Choi SK. The Effect of Specimen Size on Strength and Other Properties in Laboratory Testing of Rock and Rock-Like Cementitious Brittle

- Materials. *Rock Mech Rock Eng.* 2011;44(5):513. doi:10.1007/s00603-011-0161-6.
14. Tsur-Lavie Y, Denekamp SA. Comparison of size effect for different types of strength tests. *Rock Mech.* 1982;15(4):243-254. doi:10.1007/BF01240592.
 15. Aubertin M, Li L, Simon R. A multiaxial stress criterion for short- and long-term strength of isotropic rock media. *Int J Rock Mech Min Sci.* 2000;37(8):1169-1193. doi:10.1016/S1365-1609(00)00047-2.
 16. Mogi K. The influence of the dimensions of specimens on the fracture strength of rocks: Comparison between the strength of rock specimens and that of the earth's crust. 1962.
 17. Bieniawski ZT. Propagation of brittle fracture in rock. In: *The 10th US Symposium on Rock Mechanics (USRMS)*. American Rock Mechanics Association; 1968.
 18. Pratt HR, Black AD, Brown WS, Brace WF. The effect of specimen size on the mechanical properties of unjointed diorite. *Int J Rock Mech Min Sci.* 1972;9(4):513-516. doi:10.1016/0148-9062(72)90042-3.
 19. Medhurst TP, Brown ET. A study of the mechanical behaviour of coal for pillar design. *Int J Rock Mech Min Sci.* 1998;35(8):1087-1105. doi:10.1016/S0148-9062(98)00168-5.
 20. Hoek E, Brown T. *Underground Excavations in Rock*. Taylor & Francis; 1980. <https://books.google.co.uk/books?id=XeGKeYa8d30C>.
 21. Pierce M, Gaida M, DeGagne D. Estimation of rock block strength. In: *RockEng09 (Proceedings, 3rd CANUS Rock Mechanics Symposium, Toronto. ; 2009*.
 22. Martin CD, Lu Y, Lan H. Scale Effects in a Synthetic Rock Mass. In: *12th International Congress on Rock Mechanics of the International Society for Rock Mechanics*. International Society for Rock Mechanics; 2011:473-478.
 23. Yoshinaka R, Osada M, Park H, Sasaki T, Sasaki K. Practical determination of mechanical design parameters of intact rock considering scale effect. *Eng Geol.* 2008;96(3-4):173-186. doi:10.1016/j.enggeo.2007.10.008.
 24. Lin M, Kicker D, Damjanac B, Board M, Karakouzian M. Mechanical degradation of emplacement drifts at Yucca Mountain—A modeling case study—Part I: Nonlithophysal rock. *Int J Rock Mech Min Sci.* 2007;44(3):351-367. doi:10.1016/j.ijrmms.2006.07.011.
 25. Gao FQ, Stead D. The application of a modified Voronoi logic to brittle fracture modelling at the laboratory and field scale. *Int J Rock Mech Min Sci.* 2014;68:1-14. doi:10.1016/j.ijrmms.2014.02.003.
 26. Shin SW, Martin CD, Park ES, Christiansson R. Methodology for estimation of excavation damaged zone around tunnels in hard rock. In: *1st Canada-US Rock*

- Mechanics Symposium. American Rock Mechanics Association; 2007.
27. Lorig LJ, Watson AD, Martin CD, Moore DP. Rockslide run-out prediction from distinct element analysis. *Geomech Geoengin.* 2009;4(1):17-25. doi:10.1080/17486020902767321.
 28. Potyondy DO, Cundall PA. A bonded-particle model for rock. *Int J rock Mech Min Sci.* 2004;41(8):1329-1364.
 29. Kazerani T, Zhao J. Micromechanical parameters in bonded particle method for modelling of brittle material failure. *Int J Numer Anal Methods Geomech.* 2010;34(18):1877-1895. doi:10.1002/nag.884.
 30. Lan H, Martin CD, Hu B. Effect of heterogeneity of brittle rock on micromechanical extensile behavior during compression loading. *J Geophys Res.* 2010;115(B1):B01202. doi:10.1029/2009JB006496.
 31. Lu Y, Martin CD, Lan H. Strength of Intact Rock Containing Flaws. In: 47th US Rock Mechanics/Geomechanics Symposium. American Rock Mechanics Association; 2013.
 32. Fredrich JT, Evans B, Wong T-F. Effect of grain size on brittle and semibrittle strength: Implications for micromechanical modelling of failure in compression. *J Geophys Res.* 1990;95(B7):10907. doi:10.1029/JB095iB07p10907.
 33. Christianson M, Board M, Rigby D. UDEC simulation of triaxial testing of lithophysal tuff. In: The 41st U.S. Symposium on Rock Mechanics. ; 2006.
 34. Kazerani T, Yang ZY, Zhao J. A Discrete Element Model for Predicting Shear Strength and Degradation of Rock Joint by Using Compressive and Tensile Test Data. *Rock Mech Rock Eng.* 2011;695-709. doi:10.1007/s00603-011-0153-6.
 35. Gao F, Stead D, Kang H. Numerical investigation of the scale effect and anisotropy in the strength and deformability of coal. *Int J Coal Geol.* 2014;136:25-37. doi:10.1016/j.coal.2014.10.003.
 36. Zhang Q, Zhu H, Zhang L, Ding X. Study of scale effect on intact rock strength using particle flow modeling. *Int J Rock Mech Min Sci.* 2011;48(8):1320-1328. doi:10.1016/j.ijrmms.2011.09.016.
 37. Vallejos JA, Brzovic A, Lopez C, Bouzeran L, Ivars DM. Application of the Synthetic Rock Mass approach to characterize rock mass behavior at the El Teniente Mine, Chile. In: FLAC/DEM Symposium, Minneapolis. ; 2013.
 38. Bahrani N, Kaiser PK. Numerical investigation of the influence of specimen size on the unconfined strength of defected rocks. *Comput Geotech.* 2016;77:56-67. doi:10.1016/j.compgeo.2016.04.004.
 39. Gao FQ, Kang HP. Effects of pre-existing discontinuities on the residual strength of rock mass - Insight from a discrete element method simulation. *J Struct Geol.*

- 2016;85:40-50. doi:10.1016/j.jsg.2016.02.010.
40. Hoek E, Carranza C, Corkum B. Hoek-brown failure criterion – 2002 edition. *Narms-Tac*. 2002;267-273. doi:10.1016/0148-9062(74)91782-3.
 41. Hoek E, Martin CD. Fracture initiation and propagation in intact rock - A review. *J Rock Mech Geotech Eng*. 2014;6(4):287-300. doi:10.1016/j.jrmge.2014.06.001.
 42. Hoek E, Diederichs M. Empirical Estimation of Rock Mass Modulus.pdf - Google Drive. *Int J Rock Mech*. 2006;43(2):203-215. doi:http://dx.doi.org/10.1016/j.ijrmms.2005.06.005.
 43. Brown ET. Rock characterisation, testing and monitoring. *ISRM suggested methods*: Oxford: Pergamon Press, 1981, 211P. *Int J Rock Mech Min Sci Geomech Abstr*. 1981;18(6):109. doi:10.1016/0148-9062(81)90524-6.
 44. Hudson JA, Brown ET, Fairhurst C. Shape of the complete stress-strain curve for rock. In: *Stability of Rock Slopes*. ASCE; 1972:773-795.
 45. Jackson R, Lau JSO. The effect of specimen size on the laboratory mechanical properties of Lac du Bonnet grey granite. In: *Proceedings of the 1st International Workshop on Scale Effects in Rock Masses*, Loen, Norway. Edited by A. Pinto Da Cunha. AA Balkema, Rotterdam. ; 1990:165-174.
 46. Wasantha PLP, Ranjith PG, Zhang QB, Xu T. Do joint geometrical properties influence the fracturing behaviour of jointed rock? An investigation through joint orientation. *Geomech Geophys Geo-Energy Geo-Resources*. 2015;1(1):3-14. doi:10.1007/s40948-015-0001-3.
 47. Il'nitskaya EI. Effect of Rock-Specimen Size on Mechanical Properties in Shear Tests. by Protodyakonov, Koifman others *Isr Progr Sci Transl Jerusalem*. 1969:57-63.
 48. Pratt HR, Black AD, Brace WF. Friction and deformation of jointed quartz diorite. *Proc 3rd Congr ISRM, Denver, II-A*. 1974;306310.
 49. Tani K. Scale effect on shear strength of sedimentary soft rocks observed in triaxial compression test (influence of potential joints). In: *36th National Conference of the Japanese Geotechnical Society*. ; 2001:597-598.
 50. Liu SG, Chi Y, Wang S, LIU H, SHI A. Size effect on shear strength of basalt rock mass with columnar joints. *J Eng Geol*. 2009;17(3):367-370.
 51. Hoek E. Strength of rock and rock masses. *ISRM News J*. 1994;2(2):4-16.
 52. Saroglou H, Tsiambaos G. A modified Hoek-Brown failure criterion for anisotropic intact rock. *Int J Rock Mech Min Sci*. 2008;45(2):223-234. doi:10.1016/j.ijrmms.2007.05.004.